

INTERPRETATION OF ADJOINT SOLUTIONS FOR TURBOMACHINERY FLOWS

Sriram*, Andre Marta[†], Prem Venugopal, Brian Barr[‡] and Qiqi Wang

ABSTRACT

While the mathematical derivation of the adjoint equations and its numerical implementation is well established, there is scant discussion on the understanding of the adjoint solution by itself. As this is a field solution of similar resolution of the flow-field, there is wealth of data that can be used for design guidance. This paper addresses this specific topic. In particular, we take representative cases from turbomachinery aerodynamic problems and use the adjoint solution to identify the “physical insight” it provides. We aim to tie the adjoint solution to the flow-field which has physical properties. Towards this end, we first look at three problems 1) a fan, 2) a compressor rotor and stator, 3) a low pressure turbine. In all three of them, we focus on changes related to geometry, but one can also realize the changes using other inputs to the flow solver (eg. boundary conditions). We show how the adjoint counter-part of the density, the velocity fields and the turbulence quantities can be used to provide insights into the nature of changes the designer can induce to cause improvement in the performance metric of interest. We also discuss how to use adjoint solutions for problems with constraints to further refine the changes. Finally, we use a problem where it is not immediately apparent what geometry changes need to be used for further evaluation with optimization algorithms. In this problem, we use the adjoint and flow solution on a turbine strut, to determine the kind of end-wall treatments that reduce the loss. These changes are then implemented to show that the loss is reduced by close to 8%.

Nomenclature

α	Design Variable
\mathcal{R}	Residual Operator
ΔP_t	Drop in total pressure
ω	Specific Dissipation Rate
ψ	Adjoint Field
ρ	Density
τ_{ji}	Stress-Tensor
C	Constraint Functions
c	Convective Speed
E	Energy
I	Objective Function
inl	Inlet Quantities
k	Turbulence Kinetic Energy
l	Length of Domain
p	Pressure
P_s	Static Pressure
q	State Vector for Flow equations
T	Terminal Time
t	Time
u	Convected Quantity
u_i	Velocity Components
x_j	Coordinate direction

1 Introduction

The continuous growth of computational power has made external and internal flow simulations to be routinely performed using high-fidelity computational fluid dynamic (CFD) models. The emerging trend is to use optimization techniques as part of the design tools, with numerical design optimization becoming common practice not only in academia but also in industry.

Among the several optimization methods developed by the operations research field [14], and considering that CFD flow

*Corresponding author: shankaran@ge.com, Fluid Mechanics Lab, Global Research Center, General Electric, 1 Research Circle, Niskayuna, NY 12309, USA

[†]Center for Aerospace Science and Technology, Instituto Superior Técnico, Av. Rovisco Pais 1, 1049-001 Lisboa, Portugal

[‡]Turbomachinery Aerodynamics Lab, Global Research Center, General Electric, 1 Research Circle, Niskayuna, NY 12309, USA

Assistant Professor, Department of Aeronautics, MIT, MA, U.S.A.

simulations can take hours, if not days, to perform, the most efficient methods are gradient-based, which require a minimal number of cost function evaluations. However, these methods require an estimate of the cost function derivatives. To address this, the designer faces the problem of evaluating the derivatives [4]. Finite-difference (FD) approximations have always been popular due to their simplicity but they rapidly become computationally prohibitive when the number of variables greatly exceeds the number of functions. In this case, an adjoint method is the best-suited approach to efficiently estimate function gradients since the cost involved in calculating sensitivities using the adjoint method is therefore practically independent of the number of design variables.

The application of adjoint methods to CFD was pioneered by Pironneau [15] and it was later revisited and extended by Jameson to perform airfoil [7] and wing [8] design. More recent successful applications include multipoint aerodynamic shape optimization problems [16], aerostructural design optimization [13], and even magnetohydrodynamics flow control [11].

The major drawback of using adjoint-based gradients has always been the necessity of implementing an additional solver – the adjoint system of equations solver, that is generally of the same complexity as the flow solver. Thus, in the presence of flows modeled by the Reynolds-Averaged Navier–Stokes (RANS) equations, the corresponding adjoint system might become far too complex to be fully derived. This has led to the use of many approximations and simplifications in the implementation of such adjoint solvers. Among the different approaches found in the literature, the major ones are:

Euler equations

Both the flow and adjoint solvers only account for the inviscid flow effects. The argument being that, in some external flows, such as in clean aircraft configurations, and in some internal flows, such as in some turbine blades, the viscous effects can be neglected since there are no regions of flow separation [9].

RANS with algebraic turbulence models

The adjoint solver is consistent with the flow solver, but a simplistic turbulence model is used to expedite the development of the former solver. Often used when the viscous and turbulent effects need to be accounted for, but the development effort is kept to a minimum [6].

RANS with constant eddy viscosity (CEV) approximation

The flow solver uses proper two-equation turbulence models, such as $\kappa - \epsilon$ or $\kappa - \omega$, but the adjoint solver assumes frozen eddy viscosity. In this case, the flow is properly solved and it is assumed that the variation of viscosity can be neglected in the adjoint [18, 2].

RANS flow and adjoint solver

This corresponds to the exact derivation of the adjoint solver, regardless of the complexity of the turbulence model used.

The dual (adjoint) solver is perfectly consistent with the primal (flow) solver. This approach is made feasible if one uses the hybrid *ADjoint* methodology to develop the adjoint solver [12, 10].

These approaches are all used today by the adjoint-based design community, but there is no clear evidence of what are the penalties associated with approximation models compared to the exact adjoint solver, when using the adjoint solution to drive a realistic gradient-based optimization problem.

Traditionally the process of selecting design variations has been carried out by trial and error, relying on the intuition and experience of the designer. It is not at all likely that repeated trials using an interactive design and analysis procedure can lead to a truly optimum design. In order to take full advantage of the possibility of examining a large design space, the numerical simulations need to be combined with automatic search and optimization procedures. This can lead to automatic design methods which will fully realize the potential improvements in aerodynamic efficiency.

An approach which has become increasingly popular is to carry out a search over a large number of variations via a genetic algorithm. This may allow the discovery of (sometimes unexpected) optimum design choices in very complex multi-objective problems, but it becomes extremely expensive when each evaluation of the cost function requires intensive computation, as is the case in aerodynamic and hydrodynamic problems. Consequently, gradient-based procedures are appropriate for aerodynamic shape optimization.

2 Background

The underlying theory of adjoint-based high-fidelity CFD design optimization is presented next.

2.1 Generic Design Problem

A generic CFD design problem can be formally described as

$$\begin{aligned} & \text{Minimize } I(w, S(\alpha)) \\ & \text{w.r.t. } \alpha, \\ & \text{subject to } \mathcal{R}(\alpha, \mathbf{q}(\alpha)) = 0 \\ & C(\alpha, \mathbf{q}(\alpha)) = 0, \end{aligned} \tag{1}$$

where I is the cost function, S is the vector of design variables and w is the flow solution, which is typically a function of the design variables, and $C = 0$ represents additional constraints that may or may not involve the flow solution. The flow governing equations expressed in the form $R = 0$ also appear as a constraint, since the solution w must always obey the flow physics.

When using a gradient-based optimizer to solve the design problem (1), the evaluation of the cost and constraint functions,

and their gradients with respect to the design variables are also required, that is, $\frac{dI}{dS}$ and $\frac{dC_i}{dS}$ have to be estimated.

2.2 Flow Governing Equations

The governing equations used in the present work are the Reynolds-Averaged Navier–Stokes (RANS) equations. In conservation form, the Navier–Stokes system of equations may be written in index notation as

$$\frac{\partial \rho}{\partial t} + \frac{\partial}{\partial x_j} (\rho u_j) = 0, \quad (2a)$$

$$\frac{\partial}{\partial t} (\rho u_i) + \frac{\partial}{\partial x_j} (\rho u_i u_j + p \delta_{ij} - \tau_{ji}) = 0, \quad i = 1, 2, 3, \quad (2b)$$

$$\frac{\partial}{\partial t} (\rho E) + \frac{\partial}{\partial x_j} (\rho E u_j + p u_j - u_i \tau_{ij} + q_j) = 0, \quad (2c)$$

where ρ , u_i and E are respectively the density, mean velocity and total energy, τ_{ij} is the viscous stress and q_j is the heat flux.

A turbulence model needs to be used to model the Reynolds stresses. In this paper, a two-equation turbulence model was used, in particular the $k - \omega$ model of [19],

$$\frac{\partial}{\partial t} (\rho k) + \frac{\partial}{\partial x_j} (\rho k u_j) = \tau_{ij} \frac{\partial u_i}{\partial x_j} - \beta_k \rho k \omega + \frac{\partial}{\partial x_j} \left[\left(\mu + \sigma_k \frac{\rho k}{\omega} \right) \frac{\partial k}{\partial x_j} \right], \quad (3a)$$

$$\frac{\partial}{\partial t} (\rho \omega) + \frac{\partial}{\partial x_j} (\rho \omega u_j) = \frac{\gamma \omega}{k} \tau_{ij} \frac{\partial u_i}{\partial x_j} - \beta_\omega \rho \omega^2 + \frac{\partial}{\partial x_j} \left[\left(\mu + \sigma_\omega \frac{\rho k}{\omega} \right) \frac{\partial \omega}{\partial x_j} \right], \quad (3b)$$

where k is the turbulence kinetic energy and ω is the specific dissipation rate. The turbulent eddy viscosity is computed from $\mu_T = \rho k / \omega$ and the constants are $\gamma = 5/9$, $\beta_k = 9/100$, $\beta_\omega = 3/40$, $\sigma_k = 1/2$ and $\sigma_\omega = 1/2$. The effective viscosity used in the Navier–Stokes equations (2) is then computed as $\mu = \mu_m + \mu_T$, where μ_m is the molecular (laminar) viscosity.

In semi-discrete form, the RANS governing equations (2,3) can be expressed as

$$\frac{dq_{ijk}}{dt} + \mathcal{R}_{ijk}(\mathbf{q}) = 0, \quad (4)$$

where $\mathbf{q} = (\rho, \rho u, \rho E, \rho k, \rho \omega)^T$ is the vector of conservative variables, \mathcal{R} is the residual with all of its components (inviscid, viscous and turbulent fluxes, boundary conditions and artificial dissipation), and the triad ijk represents the three computational directions. The unsteady term of Eq.(4) is dropped out since only the steady solution of the equation is of interest in this work.

2.3 Adjoint Equations

The adjoint equations can be expressed as

$$\left[\frac{\partial \mathcal{R}}{\partial w} \right]^T \Psi = \left[\frac{\partial I}{\partial w} \right]^T, \quad (5)$$

where Ψ is the adjoint vector.

Since the CFD solver does not handle the geometric parameters α directly, but rather a computational mesh defined by the coordinates of each node \mathbf{x} , the chain rule of differentiation is used to express the gradient of the cost function with respect to the design variables as

$$\frac{dI}{d\alpha} = \frac{dI}{d\mathbf{x}} \frac{d\mathbf{x}}{d\alpha}, \quad (6)$$

being the total gradient of the cost function with respect to the grid coordinates, based on the adjoint solution Ψ , given by

$$\frac{dI}{d\mathbf{x}} = \frac{\partial I}{\partial \mathbf{x}} - \Psi^T \frac{\partial \mathcal{R}}{\partial \mathbf{x}}. \quad (7)$$

The evaluation of the gradient of each cost or constraint function in the optimization problem (1) requires solving Eq.(5) with a new right-hand side vector. On the other hand, the computational cost of the total sensitivity (7) is almost independent of the number of grid coordinates \mathbf{x} , which is the feature that makes the adjoint method so attractive for gradient-based optimization involving a large number of variables and a few functions.

2.4 Interpreting the Adjoint Solutions

The key to reading the adjoint solution is the observation that the product of the adjoint vector, Ψ , and the variation in the constraint, δR , determines the change to the objective function. This is just a re-wording of the statement that the adjoint vector is the Lagrange multiplier. However, on closer inspection, this statement can be strengthened in the context of the constraint equations being the Navier–Stokes equations. In this case, the adjoint solution at each grid point, which is a vector counter-part to the flow solution at that grid-point has a one-to-one correspondence to the flow solution. For example, the adjoint counter-part for density, can be interpreted as the change required to be induced to the density to cause an increase in the objective function of interest. Similarly the adjoint counter-part for the turbulence quantities signifies the change required in the actual turbulence quantities to increase the objective function. It is common for many problems to observe that the adjoint solution has \pm signs at different points in the computational domain. In such cases, the interpretation can be made stronger. Here, the design guidance

that the adjoint solution provides is to require that the designer cause changes that increase density where the adjoint solution is positive and decrease density where the adjoint solution is negative.

We first use the 1D constant coefficient wave equation to confirm the above statements. This equation valid over an (t, x) domain $[0, T] \times [0, l]$ along with the initial condition can be written as

$$\begin{aligned} \frac{\partial u}{\partial t} + c \frac{\partial u}{\partial x} &= 0 \\ u(0, \cdot) &= u_0 \end{aligned} \quad (8)$$

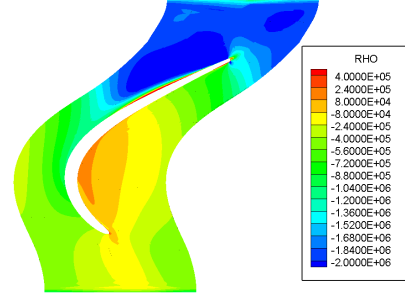
and a terminal cost function $I(T) = \int_0^l |u| dx$. The adjoint equation for $u_0 > 0 \forall x$ is

$$\begin{aligned} -\frac{\partial \psi}{\partial \tau} - c \frac{\partial \psi}{\partial x} &= 0 \\ \psi(T, \cdot) &= 1 \end{aligned} \quad (9)$$

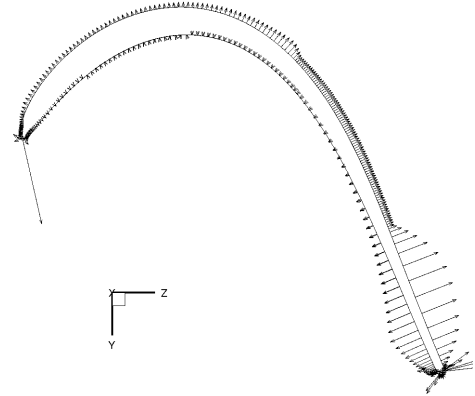
where $\tau = -t$. Hence, the adjoint solution at terminal time is a constant and it evolves backwards through a wave equation and hence remains constant over the interval $[0, T]$. Hence, the adjoint solution suggests that for all time $t = [0, T]$, the solution u , has to be increased to increase the cost function. This agrees with the form of the cost function.

If the initial condition, u_0 , varied linearly from 1 to -1 over the spatial interval (with a cross-over between positive and negative regions happening at $l/2$), then the adjoint solution for the same objective function will the solution to the backward propagating step-function whose form at time, T , has a shock at $l/2$. This would suggest that if changes are made to increase u where the adjoint solution is positive and decrease it where u is negative, then the objective function will be increased. As the objective function is an absolute function, this interpretation of the adjoint solution is also true.

A similar argument can also be used for the Burgers equation but we instead focus on the flow equations represented by Euler and Navier-Stokes equations. These equations being non-linear and in coupled form make it trickier to analyze. To ground the discussion, we take an example of a turbine vane. Figure 1 shows the contours of the adjoint variable corresponding to density for a turbine vane (the flow is from the bottom of the page to top) and the gradient vector plot on the surface of the airfoil for the Loss coefficient. The vector points in the direction of surface movement that leads to increase in Loss. The range of the adjoint solution spans the positive and negative real axis suggesting that improvements in the metric (in this case the metric is Loss which



(a) Adjoint Density Contours



(b) Gradient Vector Plot

Figure 1. 2-D vane adjoint and gradients ($d\eta/dx$).

we would like to reduce) can be obtained by decreasing the density over the suction side of the airfoil while mostly increasing it over the fore-portion of the pressure side. In relative magnitude, the suggested reduction in density near the trailing edge of the suction side is more than over the same region on the pressure side.

The Loss metric is defined as

$$\text{Loss} = \frac{\Delta P_t}{P_t^{\text{inl}} - P_s^{\text{inl}}}$$

where P_t is the total pressure and P_s is the static pressure and the super-script, inl, refers to values at the inlet. The boundary condition applied at the inlet holds the total pressure to the prescribed

value and under the assumption that the static pressure variations at the inlet are small (weak upstream travelling waves), the major contribution to the change in loss is the change to the exit total pressure. Any increase in the exit total pressure leads to an reduction in the loss metric.

If we try to make geometry changes that alter the density as suggested by the adjoint solution, the fore portion of the suction side will decelerate the flow by reducing the curvature and the mid-to-aft portion will accelerate the flow by changing the turning angle of the metal. The former will increase the density and the latter will decrease the density. On the pressure side, the suggested geometry changes pushes the axial location of the maximum pressure aft, while simultaneously providing a steeper pressure gradient in the aft portion. From a loss budget perspective, the suggested changes only lighten the possibility of shock losses and hence, the reduction in loss has to be due to the possible decrease in viscous profile losses.

With this background, we can focus on the one dimensional Euler equations. The sensitivity of the cost functional with respect to changes in the geometry can be written following Equation 7 as

$$dI = \left(\frac{\partial I}{\partial \mathbf{x}} - \psi^T \frac{\partial \mathcal{R}}{\partial \mathbf{x}} \right) d\mathbf{x}. \quad (10)$$

Now \mathcal{R} is a vector with the following elements: $\rho \cdot \hat{n}$, $(\rho u^2 + p) \cdot \hat{n}$, $\rho uH \cdot \hat{n}$. Following the earlier argument of interpreting the adjoint solution in terms of changes to the flow solution, if one manages to induce a geometry change that increases density (say) where the adjoint field for density is positive and decreases it where the adjoint field is negative, then one can achieve an overall reduction in the variation in I . Let us say that we do not a-priori know how to alter the shape, $d\mathbf{x}$ and that we can control the shape at every point in the geometry (x, y, z) . When the adjoint solution for density is positive, if we can induce a change such that the resulting flow field has a reduction in density, then the change to I (for I which does not depend on the flow field on the geometry of interest) can be written as

$$dI = \left(\frac{\partial I}{\partial \mathbf{x}} - \psi^T \frac{\partial \bar{\mathcal{R}}}{\partial \mathbf{x}} \right) d\mathbf{x} - \psi^T \frac{\partial \tilde{\mathcal{R}}}{\partial \mathbf{x}} \quad (11)$$

where $\bar{\mathcal{R}}$ is the nominal residual and $\tilde{\mathcal{R}}$ is the contribution to the residual due to reduction in density. As the residual function is linear in density, an increase in density coupled with a positive value for the adjoint density field leads to an overall increase in the variation of I . A similar argument can be made when the adjoint field is negative. Thus the change $d\mathbf{x}$ that the designer has to induce to the geometry to achieve an increase in I is that which

increases the flow density when the adjoint field is positive and decreases it when the adjoint field is negative. Similar arguments can also be made with the adjoint field for the velocities, energy and turbulence quantities through, due to the non-linearity of the Euler (or Navier-Stokes) equations, the analysis is more difficult.

This approach of interpreting the adjoint solutions is particularly useful when it is known a-priori what geometry changes will help improve the overall metric. While a similar conclusion can be drawn from investigating the gradient vector plot, interpreting the adjoint solution provides the designer a mechanism to relate the geometry changes to changes in the flow-field. Hence, it provides an intuitive feel for the designer while also allowing the designer to be cognizant of changes to other metrics that are either posed as constraints to the optimization problem or not posed at all.

3 Implementation

The development of the flow and adjoint solvers and their integration into a design system are described next.

3.1 Flow Solver

The flow solver used in this work supports three-dimensional, multi-block structured grids, it uses a finite-volume formulation of the non-linear and linear Reynolds-Averaged Navier–Stokes equations. Several turbulence models are available, such as $k - \omega$ (versions 1988,1998,2007), $k - \epsilon$ and SST, having the option to use wall functions or wall integration for boundary layer resolution. This solver is typically employed in the solution of turbomachinery blade rows and it is capable of efficiently performing three-dimensional analysis for aeromechanics, aerodynamic design, parametric studies, and robust design applications.

As typical for most iterative CFD flow solvers, the residual calculation is done in a subroutine that loops through the three-dimensional domain and accumulates the several fluxes and boundary conditions contributions in the residual \mathcal{R} . However, the residual at each computational cell only depends on the flow variables at that cell and at the cells adjacent to it, which define the stencil of dependence, as shown in Fig. 2.

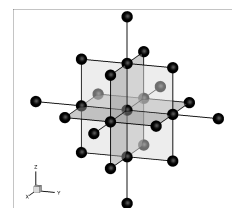


Figure 2. Computational flow stencil: 25 nodes.

3.2 Adjoint Solver

The simple mathematical form of Eq.(5) can be very misleading since, depending on the approach, their numerical implementation can be quite complex, if derived by manual differentiation, or quite costly, if derived using finite-differences.

A discrete adjoint approach formulation is chosen because it can be applied to any set of governing equations and it can treat arbitrary cost functions. As such, and in contrast to the continuous approach, no simplifications have to be made during the derivation: the effects of viscosity and heat transfer and the turbulence equations can be easily handled when deriving the discrete adjoint.

But the most interesting feature of the discrete approach is that it allows the use of automatic differentiation (AD) tools [3] in its derivation, expediting considerably the process of obtaining the differentiated form of the discretized governing equations necessary to assemble the adjoint system of equations.

As such, the approach used in this work is hybrid and it follows the work of [12] and [10] The discrete adjoint solver is derived with the aid of an automatic differentiation tool that is selectively applied to the CFD source code that handles the residual and function evaluations. This tool produces the routines that evaluate the partial derivative matrices $\partial \mathcal{R} / \partial \mathbf{q}$, $\partial Y / \partial \mathbf{q}$, $\partial Y / \partial \mathbf{x}$ and $\partial \mathcal{R} / \partial \mathbf{x}$ that are necessary to compute gradients (7) using the adjoint method (5). This hybrid approach retains the accuracy of the adjoint methods, while it adds the ease of implementation of the automatic differentiation methods. The AD tool chosen in this work is Tapenade [5] because it supports Fortran 90, which is a requirement taking into account the programming language used in the flow solver.

The sizes of the matrices involved in this process are

$$\begin{aligned} \frac{\partial \mathcal{R}}{\partial \mathbf{q}} & (N_q \times N_q) , & \frac{\partial Y}{\partial \mathbf{q}} & (N_Y \times N_q) , & (12) \\ \frac{\partial \mathcal{R}}{\partial \mathbf{x}} & (N_q \times N_x) , & \frac{\partial Y}{\partial \mathbf{x}} & (N_Y \times N_x) , \end{aligned}$$

where N_Y is the number of cost functions, N_x the number of grid coordinates and N_q the size of the state vector. The size of the vector \mathbf{q} depends on the number of governing equations, N_e , and the number of cells of the computational mesh, N_c , that discretize the physical domain, according to the relation $N_q = N_e \times N_c$, which for the solution of a large, three-dimensional problem involving a system of conservation laws, can be very large. The size of the grid coordinates vector \mathbf{x} , is given by dimensionality of the problem times the number of vertices corresponding to the computational mesh used, that is, $N_x = 3 \times N_v$ for three-dimensional problems.

The adjoint linear system of equations (5) has to be solved N_Y times because ψ is valid for all grid coordinates \mathbf{x} , but must be recomputed for each function Y . To solve this large sparse dis-

crete adjoint problem, the Portable, Extensible Toolkit for Scientific Computation (PETSc) [1] is used. The adjoint system of equations is solved using a PETSc built-in Krylov subspace method, more specifically, the Generalized Minimum Residual (GMRES) method [17].

Once the adjoint solution, ψ , is found, the gradient of the cost function with respect to the grid coordinates is obtained from Eq.(7), which implies a simple matrix-vector multiplication operation.

3.3 Constant Eddy Viscosity Approximation

The full RANS adjoint solver described so far makes use of the complete vector of conservative variables and handles the corresponding seven governing equations (2,3).

The constant eddy viscosity (CEV) approximation still solves the full RANS flow equations but it assumes that the variation of the turbulent eddy viscosity, μ_T , can be neglected in the derivation of the adjoint equations. Therefore, under de CEV assumption, only five equations (2) are used to derive the adjoint, which significantly reduces the size of the dual problem, as quantified in Eq.(12). The benefits being from easier implementation, faster run time and reduced memory requirements. The matrix $\partial \mathcal{R} / \partial \mathbf{q}$ is reduced by a factor of $7^2 / 5^2 = 1.96$, and the vector $\partial Y / \partial \mathbf{q}$ and matrix $\partial \mathcal{R} / \partial \mathbf{x}$ are reduced by a factor of $7 / 5 = 1.4$.

In the present adjoint solver implementation, a single flag controls whether CEV approximation is to be used. If so, the turbulent equations are neglected in the adjoint and the turbulent eddy viscosity is retrieved from the flow solution and added to the total adjoint viscosity.

4 Results

This section includes three examples, a commercial engine fan, a compressor rotor and stator and a low pressure turbine cascade. In each of these examples, we highlight different uses of the adjoint solution. Finally, we establish the validity of the ‘‘physical insights’’ into the adjoint solution, by using it on a turbine strut. In this case, we wish to induce end-wall treatments that result in improved performance.

4.1 Commercial Fan

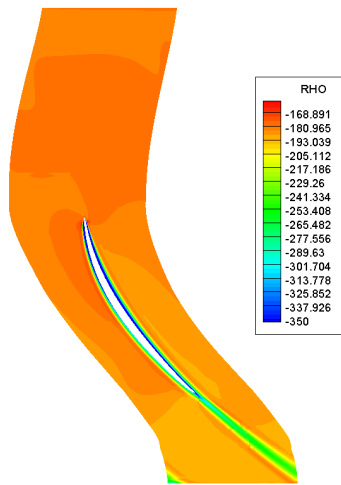


Figure 3. Contours of adjoint field for density for Efficiency. Flow is from bottom to top.

The first example is a commercial fan operating at design conditions. We are interested in adjoint solutions for the efficiency and the mass flow. The former is a performance measure we hope to improve and the latter is a constraint that we wish to respect during the design optimization. The steady state of the flow was computed using a two-equation model ($k-\omega$) and the adjoint solution was computed using the constant eddy viscosity approach. Contours of the density field of the adjoint solution for efficiency and mass flow are shown in Figures 3 and 4. These contours are roughly at mid-span. The adjoint field for efficiency suggests that geometry changes that induce larger reduction in density over the entire pressure surface. This can be achieved through a reduction in camber. On the suction surface, near the front portion of the airfoil, the necessary reduction in density is smaller (than the pressure surface). Reducing camber to accommodate the desire of the pressure surface will only lead to an increase in density over the suction surface (assuming no flow separation due to off-incidence conditions). Hence, to achieve the necessary reduction in density for the leading edge portion of the suction surface, the camber changes have to be offset by thickness increases. Towards the trailing edge, the suction and pressure surface shows a desire to reduce the density by equal amounts. These overall changes can be induced by

reducing camber for the front portion of the airfoil along with half-thickness increases to provide more curvature to the suction surface, while the portion near the trailing edge requires a combination of camber reduction and reduction in thickness.

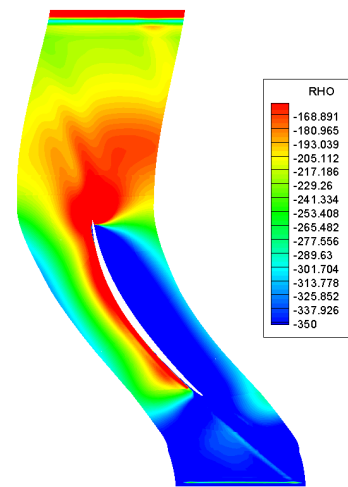


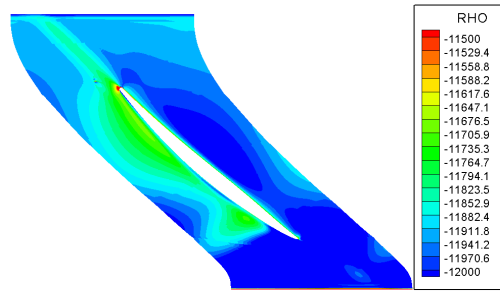
Figure 4. Contours of adjoint field for density for mass-flow. Flow is from bottom to top.

The adjoint field for mass-flow (drawn with same range as the efficiency plots for clarity) shows a trend similar to the efficiency plot. Hence, if we try to achieve higher efficiency by lowering the density for the suction surface and the pressure surface, then the mass-flow will also increase. If mass-flow is a constraint (as is typically the case to ensure fair comparison of the efficiency), then these plots suggest that room for improvement in efficiency for this section of the fan blade may be small.

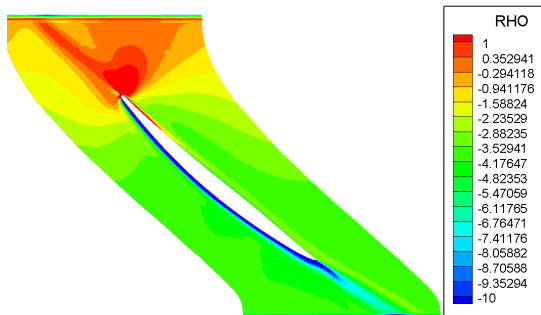
4.2 Compressor Rotor

Now we look at a compressor rotor blade. Again we look at two metrics, efficiency and pressure-ratio and the adjoint field is produced using the constant-eddy viscosity model. The pressure ratio is roughly the ratio of the pressure at the exit to the inlet of the domain. Figure 5 shows the adjoint density contours on a cut through the domain for efficiency and pressure ratio.

The range in the plot of efficiency is rather narrow and all negative on this plane. This suggests that all portions of the blade are equally sensitive to the metric of interest. On the suction surface, reduction in density is more near the leading edge region



(a) Adjoint Density for Efficiency



(b) Adjoint Density for Pressure-Ratio

Figure 5. Adjoint density contours for Efficiency and Pressure-Ratio.

and roughly around mid-chord suggesting a geometry change that increases thickness and/or camber. The plot for pressure ratio is shown on a different scale suggesting that relative to efficiency the changes in density are smaller to affect pressure ratio. The plot also suggests an overall decrease of density over the entire suction surface to cause an increase in pressure ratio.

4.3 Compressor Stator

Now we look at a compressor stator blade. Here, we only look at one metric, namely the loss. Figure 6 shows contours of the adjoint field for density. Outside the vicinity of the boundary

layer, the contours suggest that on the suction side we should increase the density to increase loss. The pressure side field suggests a similar change but of smaller magnitude. Along the boundary layer, the adjoint field suggests a decrease in density for both the pressure and suction side. This can be achieved by providing more curvature to the suction side and reducing the curvature of the pressure side. Both these changes will provide more blockage to the flow leading to higher losses.

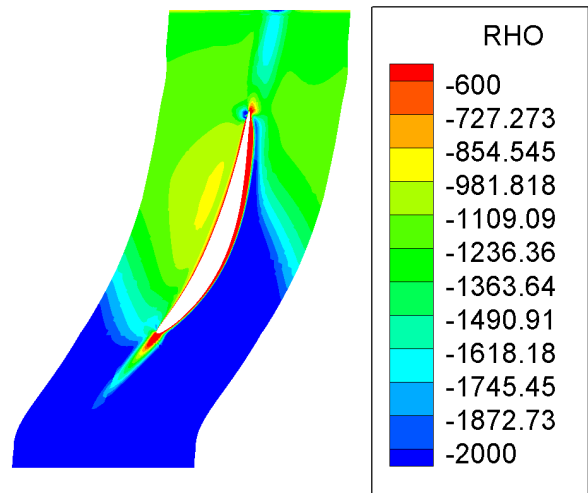
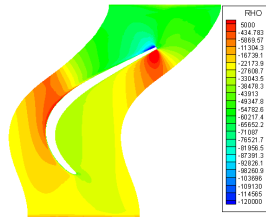


Figure 6. Contours of adjoint field for density for Loss. Flow is from bottom to top.

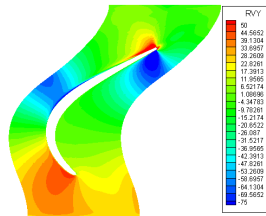
These changes are intuitive for a designer and not of immediate value for this flow. In such cases the value of the adjoint is in providing quantitative estimates of the geometrical change for use within an optimizer.

4.4 Low Pressure Turbine Vane

We have discussed this result in Section 2. Here, we focus on another metric of interest, namely the mass flow. Figure 7 shows the adjoint density and ρv_y contours for mass flow (v_y is the tangential component of velocity). These plots show three regions where increases in mass flow can be achieved. The leading edge on the suction side can contribute to increases in mass flow by increasing the camber and (or) the thickness. This will accelerate the flow even further, leading to a decrease in the density and an increase in the tangential velocity. The mid-passage



(a) Adjoint Density Contours



(b) Adjoint ρv_y Contours

Figure 7. 2-D vane adjoint solution for mass flow.

section on the suction surface can be altered to increase the mass flow by making it thinner. As suggested by the contours, this will cause the local increase in density and the decrease in local tangential velocity. Near the trailing edge, reducing the metal angle (measured from the vertical) will lead to a decrease in tangential velocity on the pressure side and a corresponding increase on the suction side. Overall, these effects can also be simulated by a variety of other geometric changes.

4.5 End-Wall Contouring

5 Conclusions

The results from this study show that it possible to derive physical understanding from the adjoint solution. Each adjoint variable quantifies the sensitivity of the corresponding conserved flux quantity in the governing Navier-Stokes equations to the metric of interest. While this is not useful for regular design problems (where the changes to be induced in the geometry are well known and what is usually unknown is the amount of change that needs to be applied) this is invaluable in the following two situations: 1) when there is scant design guidance and 2) one needs to gain some understanding into the changes in the flow-field. There are numerous instances of the former and the latter in the turbomachinery design world which will benefit from the study presented in this paper.

Acknowledgements

The authors would like to thank Daniel Wilkin, Dave Cherry and Lyle Dailey from GE Aviation, for their support and feedback. Moreover, the authors are thankful to General Electric for giving permission to publish this paper.

REFERENCES

- [1] Satish Balay, Kris Buschelman, Victor Eijkhout, William D. Gropp, Dinesh Kaushik, Matthew G. Knepley, Lois Curfman McInnes, Barry F. Smith, and Hong Zhang. PETSc users manual. Technical Report ANL-95/11 - Revision 2.3.0, Argonne National Laboratory, 2004.
- [2] Roque Corral and Fernando Gisbert. Profiled end wall design using an adjoint navier–stokes solver. *Journal of Turbomachinery*, 130(2):021011, 2008.
- [3] P. Cusdin and J.-D. Müller. On the performance of discrete adjoint CFD codes using automatic differentiation. *International Journal of Numerical Methods in Fluids*, 47(6–7):939–945, 2005.
- [4] Andreas Griewank. *Evaluating Derivatives*. SIAM, Philadelphia, 2000.
- [5] Laurent Hascoët and Valérie Pascual. Extension of TAPE-NADE towards Fortran 95. In H. M. Bücker, G. Corliss, P. Hovland, U. Naumann, and B. Norris, editors, *Automatic Differentiation: Applications, Theory, and Tools*, Lecture Notes in Computational Science and Engineering. Springer, 2005.
- [6] L. He and D. X. Wang. Concurrent blade aerodynamic-aero-elastic design optimization using adjoint method. *Journal of Turbomachinery*, 133(1):011021, 2011.
- [7] A. Jameson. Aerodynamic design via control theory. *Journal of Scientific Computing*, 3(3):233–260, September 1988.

- [8] Antony Jameson, Niles A. Pierce, and Luigi Martinelli. Optimum aerodynamic design using the Navier–Stokes equations. In *Theoretical and Computational Fluid Dynamics*, volume 10, pages 213–237. Springer-Verlag GmbH, January 1998.
- [9] Jiaqi Luo, Juntao Xiong, Feng Liu, and Ivan McBean. Three-dimensional aerodynamic design optimization of a turbine blade by using an adjoint method. *Journal of Turbomachinery*, 133(1):011026, 2011.
- [10] Charles A. Mader, Joaquim R. R. A. Martins, Juan J. Alonso, and Edwin van der Weide. ADjoint: An approach for the rapid development of discrete adjoint solvers. *AIAA Journal*, 46(4):863–873, April 2008.
- [11] A. C. Marta and J. J. Alonso. Toward optimally seeded airflow on hypersonic vehicles using control theory. *Computers & Fluids*, 39(9):1562–1574, October 2010.
- [12] A. C. Marta, C. A. Mader, J. R. R. A. Martins, E. van der Weide, and J. J. Alonso. A methodology for the development of discrete adjoint solvers using automatic differentiation tools. *International Journal of Computational Fluid Dynamics*, 21(9–10):307–327, October 2007.
- [13] Joaquim R. R. A. Martins, Juan J. Alonso, and James J. Reuther. High-fidelity aerostructural design optimization of a supersonic business jet. *Journal of Aircraft*, 41(3):523–530, May 2004.
- [14] Jorge Nocedal and Stephen J. Wright. *Numerical optimization*. Springer, 1999.
- [15] O. Pironneau. On optimum design in fluid mechanics. *Journal of Fluid Mechanics*, 64:97–110, 1974.
- [16] James J. Reuther, Juan J. Alonso, Antony Jameson, Mark J. Rimlinger, and David Saunders. Constrained multipoint aerodynamic shape optimization using an adjoint formulation and parallel computers, part 1. *Journal of Aircraft*, 36(1):51–60, 1999.
- [17] Youcef Saad and Martin H. Schultz. GMRES: A generalized minimal residual algorithm for solving nonsymmetric linear systems. *SIAM Journal for Scientific and Statistical Computing*, 7(3):856–869, July 1986.
- [18] D. X. Wang and L. He. Adjoint aerodynamic design optimization for blades in multistage turbomachines—part i: Methodology and verification. *Journal of Turbomachinery*, 132(2):021011, 2010.
- [19] D. C. Wilcox. Reassessment of the scale-determining equation for advanced turbulence models. *AIAA Journal*, 26(11):1299–1310, Nov 1988.